Article

Tracking a Low-Angle Isolated Target via an Elevation-Angle Estimation Algorithm Based on Extended Kalman Filter with an Array Antenna

Hossein Darvishi [1,*], Mohammad Ali Sebt [2], Domenico Ciuonzo [3] and Pierluigi Salvo Rossi [1]

1   Department of Electronic Systems, Norwegian University of Science and Technology, 7491 Trondheim, Norway; salvorossi@ieee.org
2   Department of Electrical Engineering, K. N. Toosi University of Technology, Tehran 15875-4416, Iran; sebt@kntu.ac.ir
3   Department of Electrical Engineering and Information Technologies (DIETI), University of Naples "Federico II", 80125 Naples, Italy; domenico.ciuonzo@unina.it
*   Correspondence: hossein.darvishi@ntnu.no; Tel.: +47-40589060

Abstract: In a low-angle tracking situation, estimating the elevation angle is challenging due to the entrance of the multipath signals in the antenna's main lobe. In this article, we propose two methods based on the extended Kalman filter (EKF) and frequency diversity (FD) process to estimate the elevation angle of a low-angle isolated target. In the first case, a simple weighting of the per-frequency estimates is obtained (termed WFD). Differently, in the second case, a matrix-based elaboration of the per-frequency estimates is proposed (termed MFD). The proposed methods are completely independent of prior knowledge of geometrical information and the physical parameters. The simulation results show that both methods have excellent performance and guarantee accurate elevation angle estimation in different multipath environments and even in very-low SNR conditions. Hence, they are both suitable for low-peak-power radars.

Keywords: array antenna; extended Kalman filter; array signal processing; target tracking; direction of arrival estimation

1. Introduction

For nearly half a century, researchers have been studying the problem of localizing low-elevation targets. Unfortunately, in the above scenario, the multipath effect causes a significant error in tracking the target elevation angle, even in the case of an isolated target. Accordingly, multipath represents the main obstacle in solving the aforementioned task accurately. Indeed, the antenna array receives more signals than one direct signal while tracking a low-angle target flying over the surface. Specifically, *specular* and *diffuse* components reflected from the surface are also received by the array and create a (ghost) image target below the surface.

These multipath components lead to an *interfering effect* in the elevation angle estimation process. Such an effect may be destructive or constructive, depending on the traveled distance from the target to the antenna and the phase difference between direct and multipath signals. However, the specular signal is more destructive due a relatively-stronger effect and higher correlation with the direct signal. Accordingly, the conventional monopulse method fails in tracking a low-angle target in the presence of multipath. To mitigate such detrimental effects, White [1] enhanced the monopulse method by introducing the double null (DN) and fixed beam (FB) methods.

These two methods were improved in [2] by squinting the antenna's sum and difference patterns. Differently, in [3], the difference monopulse pattern was designed symmetrically via beamforming. The use of the frequency diversity (FD) in an optimal way to reduce the multipath effect is investigated in [4].

An alternative algorithm resorted to the idea of using the specular reflection signal from the surface to improve the estimation accuracy of a monopulse antenna [5]. In the work [6], an iterative multipath cancellation method was devised to progressively null the reflection angle position by relying on the array antenna structure. Another iterative processing practice improved the FB method performance by adaptively steering the boresight to precisely retain a required even symmetry [7].

The complex angle method is another enhanced monopulse method, which uses the real and imaginary parts of the monopulse ratio to estimate the elevation angle [8]. The weakness of this method is that there is a large ambiguity in its angular curve. In [9], a hybrid adaptive method was proposed to exclude ambiguities from the angular curve in the estimation process by using beamforming and optimal FD. There are other super-resolution array signal processing methods, such as the multiple signal classification (MUSIC) [10], the forward–backward linear prediction [11] and the minimum norm [12].

These methods are based on the eigenvector processing and performing poorly due to high correlation between direct and reflected signals. Some proposed enhancement on these methods are aiming at improving estimation accuracy by signal decorrelation but suffering from aperture loss, an estimation bias and low cost-efficiency [13,14]. The latest methods attempted to improve the performance and reduce the very high computational load of the MUSIC method.

The first works by transforming the covariance matrix of received signals into the real-value domain by employing a unitary transform [15], and the second works by converting the two-dimensional searching into one-dimensional searching and taking advantage of the polarization smoothing and the generalized MUSIC (GMUSIC) algorithm with a polarization sensitive array system [16].

Maximum likelihood (ML) is another basic parametric estimation method that handles the signal correlation without aperture loss [17]. However, this method cannot separate the reflected signals and direct signal from each other in the low-angle situation and has high computational complexity. For suppressing the computational complexity, the beamspace domain ML method was proposed in [18].

Bosse proposed the Refined ML (RML) method to improve the ML method [19]. The RML method uses prior knowledge of the sea state and geometric information to model the specular component. The two presented methods in [20,21] were robust in terms of the fluctuation of the reflecting surface by considering the reflecting surface height as an unknown parameter. In [22], the quadrature RML (QRML) method was introduced by generating a quadrature correction term for the RML method to reduce the diffuse random component.

A method in [23] promotes the ML method over the maximum a posteriori decision and the windowing decision. In [24], a frequency-agile RML algorithm adjusts the operating frequency adaptively to minimize the mean square error (MSE) of angle estimation.

Moreover, the Kalman filter (KF), because of its feasibility, is a potent and one of the most acknowledged tools for recursive estimation of the system state [25]. The KF is used to estimate states optimally based on linear dynamical systems over normally-distributed noise [26]. The extended KF (EKF) is an extension to cope with non-linearities of the systems's dynamics, which utilizes the first-order Taylor series expansion to reinstate a linear estimation strategy [25].

A number of EKF algorithms have been proposed for angle of arrival (AoA) estimation [27–29]. Nonetheless, these algorithms are not considering the low-angle scenarios where detrimental multipath components degrade the AoA estimation performance.

In this paper, we propose two novel methods to estimate the elevation angle of a low-altitude isolated target. Our methods capitalize the EKF, as opposed to the standard KF, because of the non-linear relation between the observation and the target elevation angle. The proposed EKF estimator is able to track the elevation angle of the target by mitigating and smoothing the severe fluctuations caused by the specular and diffuse signals

by predicting the value, the velocity and the acceleration of the target elevation angle based on previous estimations.

To further increase the accuracy of the proposed methods, we rely on a FD process. In the first method, we use a (rank-based) weighting of the per-frequency angle elevation estimates. Conversely, in the second method, we use a matrix-based processing of the aforementioned per-frequency estimates via a compact representation of the multiple-measurement model.

The proposed methods can properly work in both rough and smooth surfaces and do not require prior knowledge of the target range, the surface reflection coefficient or sea state, the radar height, the polarization and the effective earth radius. The computational complexity of the proposed methods is relatively low, and yet they present significant performance in tracking low-angle targets even for a low number of antenna array elements. Still, the proposed methods show excellent performance even at very-low SNR (as opposed to other existing methods [15,16]), thus, being suitable for adoption in low-peak-powers radars.

The remainder of the manuscript is organized as follows. The propagation and multipath models are introduced in Section 2, and the proposed methods for elevation angle estimation are presented in Section 3. Section 4 presents (and discusses) the simulation results to assess the effectiveness of the proposed methods. Finally, our conclusions and future directions for research are given in Section 5.

Notation: in this paper, we use lower-case (resp. upper-case) bold letters denote vectors (resp. matrices), with a_k (resp. $a_{n,m}$) representing the kth element (resp. (n,m)th element) of a (resp. A); i is used to denote the imaginary unit; the symbols $(.)^T$ and $(.)^H$ are used to indicate transpose and conjugate transpose, respectively; I_m denotes the m-dimensional identity matrix; $\mathcal{N}(\mu, \Sigma)$ denotes a normal distribution with mean vector μ and covariance matrix Σ; Rayleigh(ρ) denotes a Rayleigh distribution with parameter ρ; $\mathcal{U}(a,b)$ denotes a uniform distribution with support (a,b); and finally, the symbols $\sim$ and $\approx$ mean "distributed as" and "approximately equal to", respectively.

2. Propagation and Multipath Models

The present section describes the propagation and multipath models considered in this work. Specifically, in Section 2.1, we first describe the general antenna array model. Then, in Section 2.2, we detail the geometric parameters involved. Finally, in Sections 2.3 and 2.4, we report the considered specular and diffuse component modeling.

2.1. General Propagation Model

As shown in Figure 1, we consider a curved-earth model with *both* specular and diffuse propagation. The considered radar is equipped with a uniform linear array (ULA) made of N elements with inter-element spacing d. The received array signal (observation) vector $x(n) \triangleq \begin{bmatrix} x_1(n) & x_2(n) & \cdots & x_N(n) \end{bmatrix}^T$, including the direct and multipath signals, is given as

$$x(n) = a(\theta_t)\,s(n) + a(\theta_r)\,s_r(n) + a(\theta_d)\,s_d(n) + w(n) \tag{1}$$

where $a(\theta) \triangleq \begin{bmatrix} 1 & e^{-ikd\sin(\theta)} & \cdots & e^{-ik(N-1)d\sin(\theta)} \end{bmatrix}^T$ denotes the steering vector, with $k = (2\pi/\lambda)$ and λ representing the wave-number and the wavelength, respectively. In Equation (1), the terms θ_t, θ_r and θ_d represent the arrival angles associated to the direct, specular and diffuse component, respectively. Analogously, $s(n)$, $s_r(n)$ and $s_d(n)$ denote the amplitudes of the direct, specular and diffuse signals, respectively. Finally, $w(n)$ is a zero-mean complex additive Gaussian observation noise vector, namely $w(n) \sim \mathcal{N}(0, C)$.

2.2. Evaluation of Geometric Parameters

According to Figure 1, the reflecting specular and diffuse signals received by the antenna array are modeled based on a curved-earth surface assumption. Consequently,

based on geometric considerations, we are able to obtain the explicit values of θ_t and θ_r, as well as that of the *grazing angle* ψ_g (which are used in the following):

$$\theta_t = \sin^{-1}\left(\frac{(r_e + h_t)^2 - R^2 - (r_e + h_r)^2}{2\,R\,(r_e + h_r)}\right) \qquad \text{(AoA direct)} \qquad (2)$$

$$\theta_r = \sin^{-1}\left(\frac{h_r}{R_1} + \frac{R_1}{2\,r_e}\right) \qquad \text{(AoA specular)} \qquad (3)$$

$$\psi_g = \sin^{-1}\left(\frac{h_r}{R_1} - \frac{R_1}{2\,r_e}\right) \qquad \text{(grazing angle)} \qquad (4)$$

where h_r and h_t are the radar and target heights, respectively. Additionally, r_e denotes the effective earth's radius, which equals $4/3$ times the earth's radius ($\approx 8504\,\text{km}$). Furthermore, R, R_1 and R_2 represent (*a*) the radar to target range, (*b*) the radar to the surface reflection point range and (*c*) the reflection point to target range, respectively. Finally, r_1 and r_2 are the corresponding *surface distances* of R_1 and R_2. Such distance pairs can be obtained through the following formulas:

$$R_1 = \left(r_e^2 + (r_e + h_r)^2 - 2r_e(r_e + h_r)\cos(r_1/r_e)\right)^{1/2} \qquad (5)$$

$$R_2 = \left(r_e^2 + (r_e + h_t)^2 - 2r_e(r_e + h_t)\cos(r_2/r_e)\right)^{1/2} \qquad (6)$$

$$r_1 = r_e \sin^{-1}\left(\sqrt{\frac{R^2 - (h_t - h_r)^2}{4\,(h_r + r_e)\,(h_t + r_e)}}\right) - f\,\sin(\eta/3) \qquad (7)$$

$$r_2 = r_e \sin^{-1}\left(\sqrt{\frac{R^2 - (h_t - h_r)^2}{4\,(h_r + r_e)\,(h_t + r_e)}}\right) + f\,\sin(\eta/3) \qquad (8)$$

where $f \triangleq \frac{2}{\sqrt{3}}\left(r_e(h_t + h_r) + \frac{(r_1+r_2)^2}{4}\right)^{1/2}$ and $\eta \triangleq \sin^{-1}\left(\frac{2\,r_e(r_1+r_2)\,(h_t-h_r)}{f^3}\right)$ are suitably-defined auxiliary coefficients. The aforementioned set of formulas for the evaluation of radar-target geometric parameters are leveraged in what follows to model the specular and diffuse components.
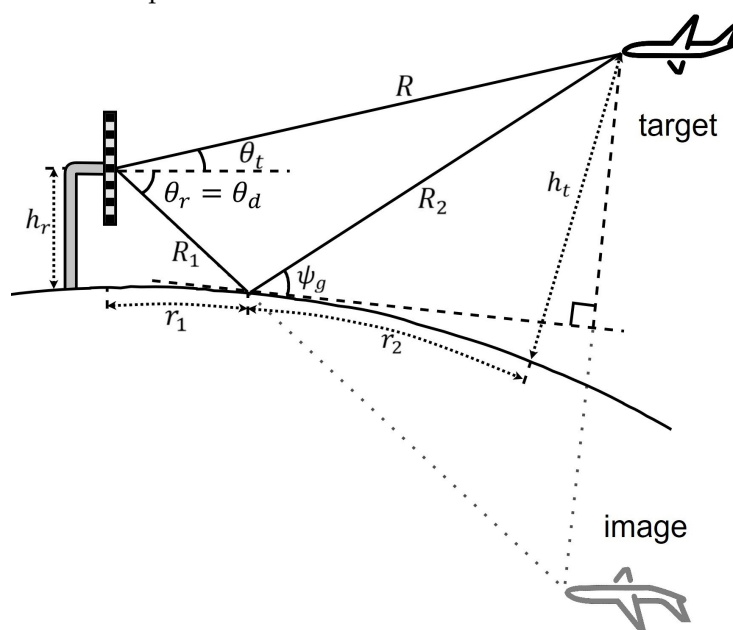
Figure 1. Multipath geometry model.

2.3. Specular Component Modeling

In this study, we model the *specular* component as follows

$$s_r(n) = \Gamma \, D \, \rho_s \, e^{-i\Delta\phi} s(n) \qquad (9)$$

where Γ is the Fresnel reflection coefficient, D is the divergence coefficient, ρ_s is the specular scattering coefficient, and $\Delta\phi$ denotes the phase lag. We now provide details for each of these constituting parameters.

The *Fresnel reflection coefficient*, which determines the ratio of the signal amplitude after and before the incidence on a surface, is given for either vertical and horizontal polarization as follows [30]

$$\Gamma = \begin{cases} \dfrac{\varepsilon_c \sin(\psi_g) - \sqrt{\varepsilon_c - \cos^2(\psi_g)}}{\varepsilon_c \sin(\psi_g) + \sqrt{\varepsilon_c - \cos^2(\psi_g)}} & \text{vertical polarization} \\[2ex] \dfrac{\sin(\psi_g) - \sqrt{\varepsilon_c - \cos^2(\psi_g)}}{\sin(\psi_g) + \sqrt{\varepsilon_c - \cos^2(\psi_g)}} & \text{horizontal polarization} \end{cases} \qquad (10)$$

We observe that the coefficient Γ is a function of (*a*) the grazing angle ψ_g and (*b*) the surface dielectric coefficient ε_c. The latter parameter is expressed as $\varepsilon_c = \varepsilon - i60\lambda\sigma$, where ε is the dielectric constant and σ is the conductivity. Such dependence makes Γ a frequency-dependent parameter.

Conversely, the *divergence factor*, accounting for the incidence of the signal on a curved earth surface, can be expressed approximately as

$$D \approx \frac{1}{\sqrt{\left(1 + \dfrac{2r_1 r_2}{r_e(r_1 + r_2)\sin(\psi_g)}\right)}} \qquad (11)$$

where r_1 and r_2 are surface distances of R_1 and R_2 (cf. Equations (5)–(8)), respectively. We can extract the angles with respect to the curved earth and propagation model in Figure 1.

Furthermore, we use Northam's model [31] for accurately calculating the *specular scattering coefficient*, namely:

$$\rho_s = \begin{cases} e^{-2(2\pi g)^2} & 0 \le g \le 0.1 \\[2ex] \dfrac{0.812537}{1 + 2(2\pi g)^2} & g > 0.1 \end{cases} \qquad (12)$$

where $g = (\sigma_h \sin(\psi_g)/\lambda)$ denotes the surface roughness coefficient, which depends on both the RMS of the surface roughness σ_h and the grazing angle ψ_g.

Finally, the *phase lag* functional expression is $\Delta\phi = -k(R - (R_1 + R_2))$. The latter quantity depends on the radar to target range (R), the radar to the surface reflection point range (R_1) and the reflection point to target range (R_2).

2.4. Diffuse Component Modeling

According to Beard's experimental data [32], the random *diffuse* component can be adequately modeled by considering its reflection point at the specular reflection point (i.e., $\theta_r = \theta_d$).

Hence, the vector component associated to the diffuse signal is given as:

$$a(\theta_d)\, s_d(n) \approx a(\theta_r)\, \rho_d \, s(n) \qquad (13)$$

where ρ_d is used to indicate the (complex-valued) diffuse reflection coefficient. The latter parameter is modeled as a circularly-complex valued Gaussian random variable [31,33].

Thus, the diffuse coefficient ρ_d can be equivalently expressed in the form $\rho_d = a_d\, e^{i\varphi_d}$, where $a_d \sim \text{Rayleigh}(\sigma_d)$ and $\varphi_d \sim \mathcal{U}(0, 2\pi)$, respectively. In the considered diffuse amplitude model, the Rayleigh parameter σ_d assumes the following expression

$$\sigma_d \triangleq \begin{cases} 3.68\sqrt{2}\,|\Gamma|\,g & 0 < g < 0.1 \\ \sqrt{2}\,|\Gamma|(0.454 - 0.858\,g) & 0.1 \leq g < 0.5 \\ 0.025\sqrt{2}\,|\Gamma| & g \geq 0.5, \end{cases} \tag{14}$$

which depends on both the surface roughness coefficient (g) and the Fresnel reflection coefficient (Γ).

To gain insight on the relative importance of specular and diffuse components in different scenarios, Figure 2 illustrates the specular scattering coefficient ρ_s and the Rayleigh parameter σ_d for different surface roughness conditions at an antenna height of 15 m. The considered target is assumed to be fixed at range 20 km and altitude 80 m. Specifically, in *smooth surfaces* ($g < 0.1$), the specular component has strong power, and the specular scattering coefficient reaches a unit value whereas the Rayleigh parameter of the diffuse component peak value equals 0.5, thus, showing that the specular signal has a more destructive effect. Therefore, this demonstrates that the angle error on the smooth surface is greater than the *rough surface* ($0.1 < g < 0.5$).
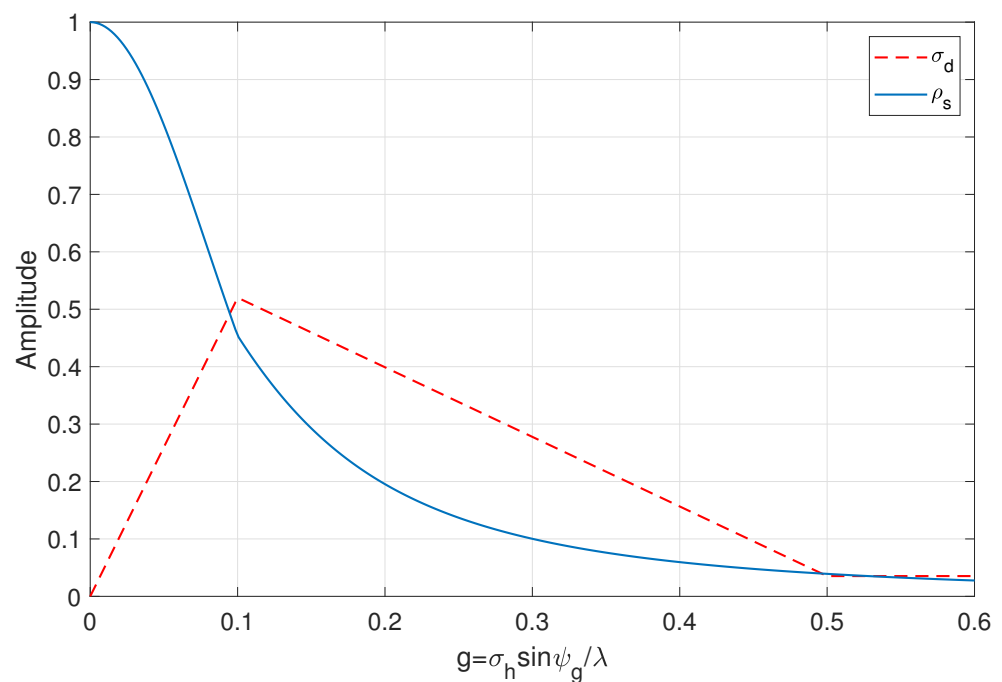
Figure 2. The specular scattering coefficient and Rayleigh parameter against the surface roughness.

3. Elevation Angle Estimation

This section describes the proposed methodology for low-angle tracking in multipath conditions. First, in Section 3.1, the EKF filter is derived, and the problem of unknown parameters is tackled. Then, in Section 3.2, the capitalization of FD is explained, and the fusion of per-frequency estimates is integrated within the considered EKF workflow.

3.1. EKF-Based Tracking

In this section, we propose an EKF method for low-elevation-angle estimation. The (linear) KF is not valid for the low-angle target estimation because the observation relation with the elevation angle in Equation (1) is nonlinear. As mentioned earlier, we also use the predictions of the velocity $\dot{\theta}_t(n)$ and the acceleration $\ddot{\theta}_t(n)$ of target elevation angle to improve the estimation accuracy. Accordingly, the state vector considered herein is

$\boldsymbol{\theta}_t(n) \triangleq \begin{bmatrix} \theta_t(n) & \dot{\theta}_t(n) & \ddot{\theta}_t(n) \end{bmatrix}^T$. The considered state-evolution and measurement models are summarized as follows

$$\begin{cases} \boldsymbol{\theta}_t(n) &= \boldsymbol{A}\boldsymbol{\theta}_t(n-1) + \boldsymbol{B}\boldsymbol{u}(n) \\ \boldsymbol{x}(n) &= \boldsymbol{h}(\boldsymbol{\theta}_t(n)) + \boldsymbol{w}(n) \end{cases} \tag{15}$$

where $\boldsymbol{u}(n) \sim \mathcal{N}(\boldsymbol{0}, \boldsymbol{Q})$ denotes the system (viz. process) noise (assumed to be independent from sample to sample) and

$$\boldsymbol{A} \triangleq \begin{bmatrix} 1 & T & \frac{1}{2}T^2 \\ 0 & 1 & T \\ 0 & 0 & 1 \end{bmatrix} \qquad\qquad \boldsymbol{B} \triangleq \begin{bmatrix} \frac{1}{2}T^2 & T & 1 \end{bmatrix}^T \tag{16}$$

In the above definitions, the term T represents the sampling period. Conversely, $\boldsymbol{h}(\cdot)$ denotes the N-dimensional measurement mapping, expressed in Equation (1), which relates θ_t (i.e., the elevation angle of the target) to the noise-free received signal vector. Hence, the observation vector does not (explicitly) contain the velocity ($\dot{\theta}_t$) and the acceleration ($\ddot{\theta}_t$) of the elevation angle. Finally, $\boldsymbol{w}(n)$ is the measurement noise vector as defined in Equation (1).

Thus, the prediction equation for obtaining $\hat{\boldsymbol{\theta}}_t(n|n-1)$ and the corresponding minimum prediction MSE matrix $\boldsymbol{M}(n|n-1)$ can be expressed as

$$\hat{\boldsymbol{\theta}}_t(n|n-1) = \boldsymbol{A}\,\hat{\boldsymbol{\theta}}_t(n-1|n-1) \tag{17}$$

$$\boldsymbol{M}(n|n-1) = \boldsymbol{A}\,\boldsymbol{M}(n-1|n-1)\,\boldsymbol{A}^T + \boldsymbol{B}\boldsymbol{Q}\boldsymbol{B}^T \tag{18}$$

where $\hat{\boldsymbol{\theta}}_t(n-1|n-1)$ and $\boldsymbol{M}(n-1|n-1)$ are the final (elevation angle) target vector estimate at previous sample and the corresponding MSE matrix, respectively. Both these quantities are obtained based on the correction step driven by the considered measurement model. Regarding such a model, we first analyze, in what follows, the single-frequency (narrowband) case. Then, in Section 3.2, we generalize the correction step to the multi-frequency case.

Starting from Equation (1), we ignore at the design phase the unknown terms $\boldsymbol{a}(\theta_r)\,s_r(n)$ and $\boldsymbol{a}(\theta_d)\,s_d(n)$, and we approximate the (non-linear) function $\boldsymbol{h}(\cdot)$ by linearizing it around the current estimate. In order to do so, we resort to the calculation of the Jacobian matrix of the mapping $\boldsymbol{h}(\cdot)$ w.r.t. the state vector $\boldsymbol{\theta}_t(n)$, denoted with $\boldsymbol{H}(n)$:

$$\boldsymbol{H}(n) \triangleq \left.\frac{\partial \boldsymbol{h}(\cdot)}{\partial \boldsymbol{\theta}_t(n)}\right|_{\theta_t(n)=\hat{\theta}_t(n|n-1)} = s(n) \left.\frac{\partial \boldsymbol{a}(\cdot)}{\partial \boldsymbol{\theta}_t(n)}\right|_{\theta_t(n)=\hat{\theta}_t(n|n-1)} \tag{19}$$

$$= s(n) \left.\begin{bmatrix} 0 & 0 & 0 \\ e^{-ikd\sin(\theta_t(n))}(-ikd\cos(\theta_t(n))) & \vdots & \vdots \\ \vdots & \vdots & \vdots \\ e^{-ik(N-1)d\sin(\theta_t(n))}(-ik(N-1)d\cos(\theta_t(n))) & 0 & 0 \end{bmatrix}\right|_{\theta_t(n)=\hat{\theta}_t(n|n-1)} \tag{20}$$

We recall that $\boldsymbol{H}(n)$ is an $N \times 3$-dimensional matrix. Additionally, from inspection of $\boldsymbol{h}(\cdot)$, the observation does not contain the velocity and the acceleration of the elevation angle. Hence, the second and third columns of $\boldsymbol{H}(n)$ are always null. From inspection of Equation (19), it is apparent that the presence of the unknown scattering parameter $s(n)$ precludes the exact calculation of both $\boldsymbol{h}(n)$ and $\boldsymbol{H}(n)$ at each time step n. Accordingly, we propose to use $\hat{\boldsymbol{h}}(n)$ and $\hat{\boldsymbol{H}}(n)$, where $s(n)$ is replaced by a corresponding suitable estimate $\hat{s}(n)$.

Specifically, given the received array signal $x(n)$, we can estimate the complex amplitude of the direct signal from the following least squares (LS) problem

$$\hat{s}(n) \triangleq \arg\min_{s(n)} \| x(n) - a(\theta_t(n)) s(n) \|^2 \tag{21}$$

Thus, the estimated complex amplitude of the direct signal $\hat{s}(n)$ is obtained in closed form as

$$\hat{s}(n) = \left[a(\theta_t(n))^H a(\theta_t(n)) \right]^{-1} a(\theta_t(n))^H x(n) \Big|_{\theta_t(n) = \hat{\theta}_t(n|n-1)} \tag{22}$$

In the above equation, the unknown AoA $\theta_t(n)$ is in turn replaced with the corresponding prediction one-step prediction $\hat{\theta}_t(n|n-1)$. As a result, the equations of Kalman gain matrix $K(n)$, correction (estimation) $\hat{\theta}_t(n|n)$ and filtering MSE matrix $M(n|n)$ for the complex-valued EKF are given as [34]

$$K(n) = M(n|n-1)\, \hat{H}^H(n) \left[C + \hat{H}(n)\, M(n|n-1)\, \hat{H}^H(n) \right]^{-1} \tag{23}$$

$$\hat{\theta}_t(n|n) = \hat{\theta}_t(n|n-1) + \Re\left\{ K(n) \left[x(n) - \hat{h}\big(\hat{\theta}_t(n|n-1); n\big) \right] \right\} \tag{24}$$

$$M(n|n) = \left[I_3 - K(n)\, \hat{H}(n) \right] M(n|n-1) \tag{25}$$

where I_3 is the 3×3 identity matrix, and C is the observation noise covariance matrix.

3.2. Proposed FD-Based Smoothing

When capitalizing the diversity arising from wideband processing, *multiple measurements (at different frequencies)* are available for the direct AoA $\theta_t(n)$ at the same time. Accordingly, the state-evolution and measurement models generalize as follows:

$$\begin{cases} \theta_t(n) &= A\theta_t(n-1) + Bu(n) \\ x_f(n) &= h_f(\theta_t(n)) + w_f(n), \quad f = 1, \dots F \end{cases} \tag{26}$$

where $f = 1, \dots, F$ is used to denote the frequency bins, with F being the total number of frequencies considered. The above measurement model at different frequencies can be also collected in compact form as follows:

$$\begin{cases} \theta_t(n) &= A\theta_t(n-1) + Bu(n) \\ x_{\text{fd}}(n) &= h_{\text{fd}}(\theta_t(n)) + w_{\text{fd}}(n), \end{cases} \tag{27}$$

where we have used the definitions $x_{\text{fd}}(n) \triangleq \left[x_1(n)^T \cdots x_F(n)^T \right]^T$, $w_{\text{fd}}(n) \triangleq [w_1(n)^T \cdots w_F(n)^T]^T$ and $h_{\text{fd}}(\cdot) = \left[h_1(\cdot)^T \cdots h_F(\cdot)^T \right]^T$, respectively.

Herein, we first observe that, with respect to the single-frequency case, the *prediction step is unvaried*, i.e.,

$$\hat{\theta}_t(n|n-1) = A\, \hat{\theta}_t(n-1|n-1) \tag{28}$$

$$M(n|n-1) = A\, M(n-1|n-1)\, A^T + BQB^T \tag{29}$$

Conversely, in the following we present two FD-based methods for improving the performance of the *correction step*. Specifically, one relies on simple weighting of per-frequency elevation estimates (WFD), whereas the other provides a matrix-based elaboration of the aforementioned estimates (MFD). The final elevation-angle estimate provided by the proposed FD-based methods has very high accuracy due to smoothing and the multipath mitigation effect. This is achieved due to the combined use of EKF-based tracking (which leverages the time-dependence of the AoA) and multiple-frequency capitalization.

3.2.1. Smoothing via Weighting-Based Frequency Diversity (WFD)

In the first approach, we arrange the estimated elevation angles for all frequencies by *increasing magnitude*, namely

$$\hat{\theta}_t^{(1)}(n|n) \leq \hat{\theta}_t^{(2)}(n|n) \leq \cdots \leq \hat{\theta}_t^{(F)}(n|n) \tag{30}$$

After that, we multiply each of these angles (as well as its corresponding MSE matrix M_f) by an appropriate weighting coefficient and add them [4]. By doing so, we can eliminate large peak errors by always giving the lowest proportion to the largest elevation angle estimation. On the other hand, intermediate estimations have lower error probabilities. Then, weighting by rank is expected to yield better estimate performance than a simple average. The rank-based weighting formula considered in this work is the following

$$r_m = \frac{2(F - m)}{F(F + 1)} \tag{31}$$

where r_1 (resp. r_F) represents the biggest (resp. smallest) coefficient. Accordingly, we assign these coefficients and derive the final angle estimation ($\hat{\theta}_t^{\text{wfd}}$) and averaged MSE matrix (M^{wfd}) as follows

$$\hat{\theta}_t^{\text{wfd}} = \begin{cases} r_{F-1}\hat{\theta}_t^{(1)} + \cdots + r_2\hat{\theta}_t^{(\frac{F}{2}-1)} + r_1\hat{\theta}_t^{(\frac{F+1}{2})} + r_3\hat{\theta}_t^{(\frac{F}{2}+1)} + \cdots + r_F\hat{\theta}_t^{(F)} & \text{for odd } F \\ r_{F-1}\hat{\theta}_t^{(1)} + \cdots + r_1\hat{\theta}_t^{(\frac{F}{2})} + r_2\hat{\theta}_t^{(\frac{F+1}{2})} + \cdots + r_F\hat{\theta}_t^{(F)} & \text{for even } F \end{cases} \tag{32}$$

$$M^{\text{wfd}} = \begin{cases} r_{F-1}M^{(1)} + \cdots + r_2 M^{(\frac{F}{2}-1)} + r_1 M^{(\frac{F+1}{2})} + r_3 M^{(\frac{F}{2}+1)} + \cdots + r_F M^{(F)} & \text{for odd } F \\ r_{F-1}M^{(1)} + \cdots + r_1 M^{(\frac{F}{2})} + r_2 M^{(\frac{F+1}{2})} + \cdots + r_F M^{(F)} & \text{for even } F \end{cases} \tag{33}$$

where $M^{(f)}$, $f = 1, \ldots, F$ is the filtering MSE matrix at fth frequency (after re-ordering). For brevity, we have used the short-hand notations $\hat{\theta}_t^{(f)}(n|n) \rightarrow \hat{\theta}_t^{(f)}$ and $M^{(f)}(n|n) \rightarrow M^{(f)}$ in the above two formulas. Finally, the final angle estimation $\hat{\theta}_t^{\text{wfd}}$ and averaged MSE matrix M^{wfd} are used to update the prediction step (cf. Equations (28) and (29)) for the next time step.

3.2.2. Smoothing via Matrix-Based Frequency Diversity (MFD)

In such a case, the update step in the presence of FD is obtained by the following *set of correction equations* exploiting the compact representation reported in Equation (27):

$$K^{\text{mfd}}(n) = M(n|n-1)\,\hat{H}_{\text{fd}}^H(n)\left[C_{\text{fd}} + \hat{H}_{\text{fd}}(n)\,M(n|n-1)\,\hat{H}_{\text{fd}}^H(n)\right]^{-1} \tag{34}$$

$$\hat{\theta}_t^{\text{mfd}}(n|n) = \hat{\theta}_t(n|n-1) + \Re\left\{K^{\text{mfd}}(n)\left[x_{\text{fd}}(n) - \hat{h}_{\text{fd}}(\hat{\theta}(n|n-1); n)\right]\right\} \tag{35}$$

$$M^{\text{mfd}}(n|n) = \left[I_3 - K_{\text{fd}}(n)\,\hat{H}_{\text{fd}}(n)\right]M(n|n-1) \tag{36}$$

Analogously, the final angle estimation $\hat{\theta}_t^{\text{mfd}}$ and filtering MSE matrix M^{mfd} are used to update the prediction step (cf. Equations (28) and (29)) for the next time step. In the above formulation, we capitalized the stacked observation covariance matrix, e.g., $C_{\text{fd}} = \text{diag}(C_1, \ldots, C_F)$ and the stacked non-linear mapping and Jacobian matrix. The former is clearly equal to:

$$h_{\text{fd}}(n) = \begin{bmatrix} s(n,1)\,a_1(\theta_t(n)) \\ \vdots \\ s(n,F)\,a_F(\theta_t(n)) \end{bmatrix}\Bigg|_{\theta_t(n)=\hat{\theta}_t(n|n-1)} \tag{37}$$

whereas the latter is given as:

$$
\boldsymbol{H}_{\text{fd}}(n) = \left. \begin{bmatrix} s(n,1)\frac{\partial \boldsymbol{a}_1(\theta_t(n))}{\partial \theta_t(n)} & 0 & 0 \\ \vdots & \vdots & \vdots \\ s(n,F)\frac{\partial \boldsymbol{a}_F(\theta_t(n))}{\partial \theta_t(n)} & 0 & 0 \end{bmatrix} \right|_{\theta_t(n)=\hat{\theta}_t(n|n-1)}
\tag{38}
$$

Since the signal over different frequencies is *unknown*, a similar approximation can be performed by plugging the estimates $\hat{s}(n,f)$ in $\boldsymbol{H}_{\text{fd}}(n)$ and $\boldsymbol{h}_{\text{fd}}(n)$, obtained as:

$$
\hat{s}(n,f) = \left. \left[\boldsymbol{a}_f(\theta_t(n))^H \boldsymbol{a}_f(\theta_t(n)) \right]^{-1} \boldsymbol{a}_f(\theta_t(n))^H \boldsymbol{x}_f(n) \right|_{\theta_t(n)=\hat{\theta}_t(n|n-1)}
\tag{39}
$$

Capitalizing the above estimates provides the quantities $\hat{\boldsymbol{H}}_{\text{fd}}(n)$ and $\hat{\boldsymbol{h}}_{\text{fd}}(n)$, respectively.

4. Simulation Results

In this section, we evaluate the tracking performance of the proposed approach via simulations. In detail, a moving target from 5 to 20 km at 80 m altitude is considered. The target emits a constant signal during the whole observation window. The noise vector is assumed as $\boldsymbol{w}(n) \sim \mathcal{N}(\boldsymbol{0}, \sigma_c^2 \boldsymbol{I}_N)$. Two multipath environments are considered to examine the proposed method at a satisfactory depth: (*i*) a smooth surface scenario (with dominance of the specular reflection) and (*ii*) a rough surface (with dominance of the diffuse reflection). The SNR is set to 10 dB, and five operational frequencies for the WFD process are considered, taken around the center frequency of 15 GHz. The sampling period equals $T = 0.01$ s. The process noise vector within EKF is modeled as $\boldsymbol{u}(n) \sim \mathcal{N}(\boldsymbol{0}, \sigma_q^2 \boldsymbol{I}_N)$, where $\sigma_q = 0.005$.

The ULA with the 15 m height is made of $N = 10$ elements positioned vertically and spaced by the center wavelength. The number of the snapshots used in the simulations is 10 for each frequency and the number of Monte Carlo trials is 100. More details about the antenna specifications and environment parameters are listed in Table 1.

Table 1. Antenna specifications and environment parameters.

Parameter	Value
Number of antenna elements (N)	10
Antenna height (h_r)	15 m
Target height (h_t)	80 m
Operating frequencies	$\{14, 14.5, 15, 15.5, 16\}$ GHz
Number of snapshots (S)	10
Beamwidth (θ_{3dB})	11.45°
Polarization	Horizontal
SNR	10 dB
RMS of surface roughness (σ_h)	0.2 m (smooth surface)
	0.8 m (rough surface)
Dielectric constant (ϵ)	80.1
Surface conductivity (σ)	4.8 mho/m

We compare the proposed FD-based methods with the double unitary transform based GMUSIC (DU-GMUSIC) and the polarization smoothing GMUSIC (PS-GMUSIC) methods [15,16]. Since both methods require a high number of snapshots to estimate the covariance matrix of received signals accurately, $S = 256$ snapshots are considered. In what follows, we first focus on one instance of the considered trajectory, i.e., by analyzing only a single realization of the measurement noise.

As shown in Figure 3a,b, the proposed methods are tracking very accurately the (true) target elevation angle in both smooth and rough surfaces. Indeed, both the proposed approaches suppress the diffuse fluctuations very well based on EKF smoothing ability and with the capitalization of FD.

(a)

(b)
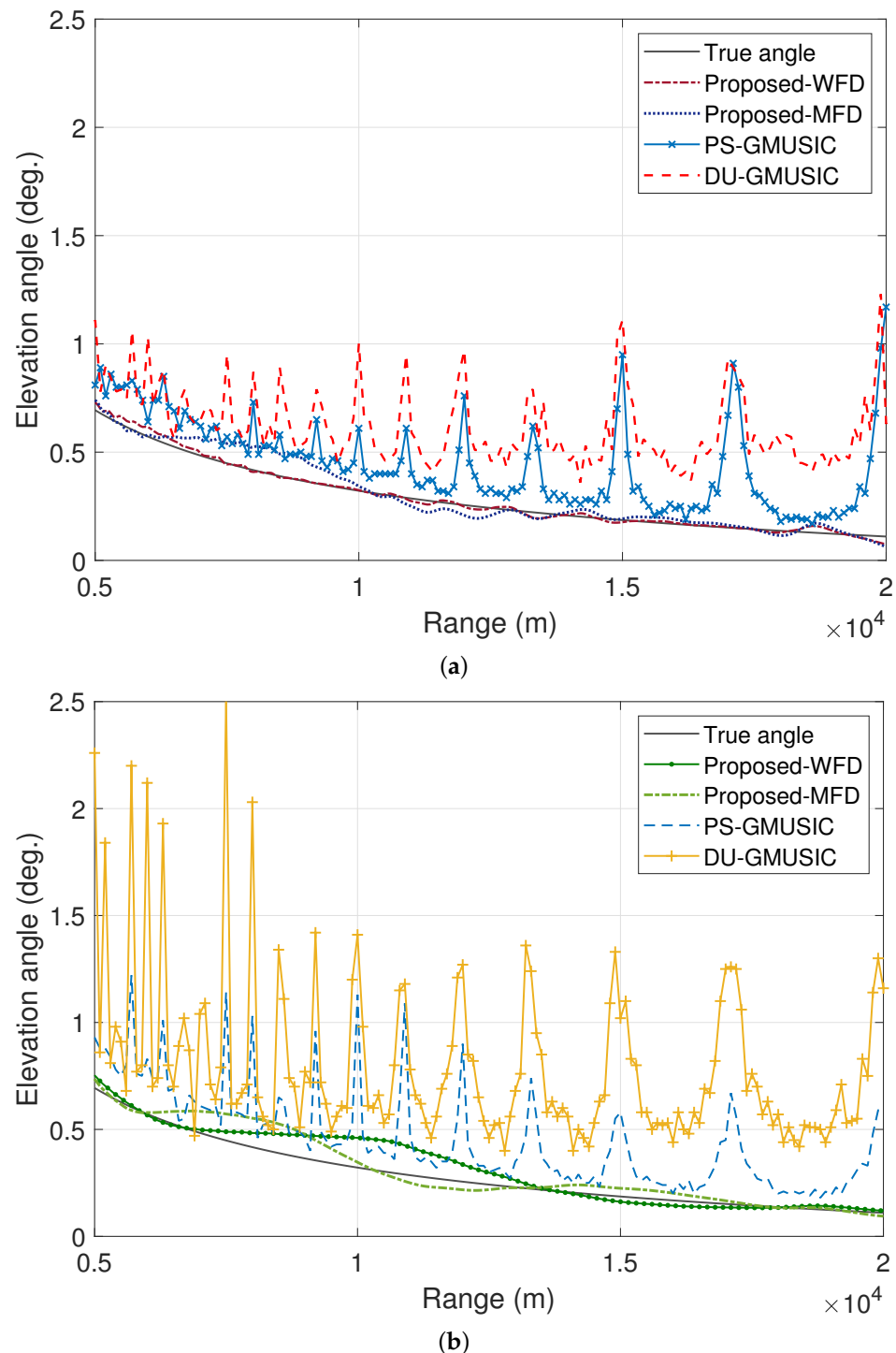
Figure 3. The target elevation angle (θ_t) estimation versus the target range. (**a**) Smooth surface. (**b**) Rough surface.

As depicted in Figure 4a,b, the proposed methods are also capable of providing explicit velocity and acceleration estimates of the elevation angle. Conversely, MUSIC-based baselines (PS-GMUSIC and DU-GMUSIC) are not designed to estimate the velocity/acceleration

explicitly. For the sake of a complete comparison, we obtained their velocity/acceleration estimates as the first derivative of the angle estimates at consecutive time indices. Accordingly, the proposed methods are tracking the velocity/acceleration in a relatively-accurate fashion in both surfaces and over all the trajectory, while the other two competitor methods are providing out-of-scale velocity/acceleration estimates.
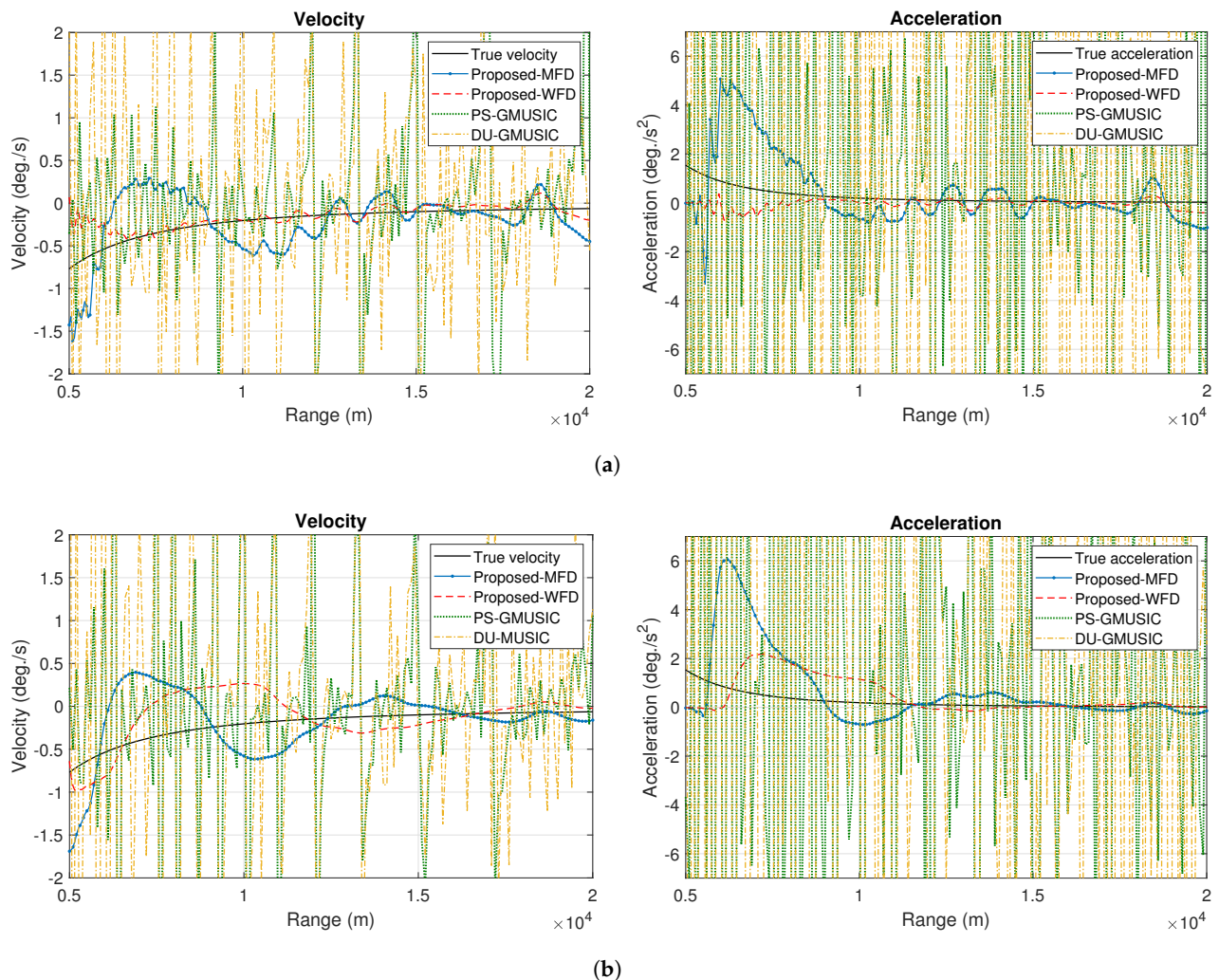
Figure 4. Velocity ($\dot{\theta}_t$) and acceleration ($\ddot{\theta}_t$) estimation of target elevation angle versus the target range. (**a**) Smooth surface. (**b**) Rough surface.

To provide a complementary (finer-grained) error analysis, Figure 5a,b reports the scatter plots for the elevation angle estimate, which obtained over 100 Monte Carlo runs of the same trajectory. As apparent from the results, the estimates for each range bin are mostly distributed around the true angle for both the proposed methods, with insignificant outlier points. Accordingly, the proposed estimators exhibit both a negligible bias and a very limited variance. As expected, proposed methods performed better over rough surfaces than over smooth ones. Indeed, the latter causes a stronger reflection power (according to Figure 2). On the contrary, both PS-GMUSIC and DU-GMUSIC present highly-biased angle estimates with a significant (higher) standard deviation.

To assess the estimation accuracy of the elevation angle estimation, we now assess it via the well-known root mean square error (RMSE). Specifically, Figure 6 shows the RMSE of the proposed method, which is much lower than (about one tenth of) the RMSE of the DU-GMUSIC and PS-GMUSIC methods in both cases (smooth and rough surfaces). Accordingly, the error of the proposed methods is negligible. However, the other two com-

petitors use more snapshots than the proposed method, but they are unable to track the target with respect to their severe fluctuations in estimation caused by the multipath effect.

The performance of these methods are degraded in the very-low angle situation. Then, to stress the performance of the proposed approaches in a wide range of relevant scenarios, Figures 7 and 8 represent their performance against the SNR and the number of snapshots, respectively. First, by looking at Figure 7, the proposed method shows the excellent performance in tracking the low-angle targets. The performance of both proposed methods, even at very-low SNR, are appreciably higher (viz. lower in terms of RMSE) with respect to the other two (MUSIC-based) baselines considered.

As a result, the proposed FD-based methods can be used in very-low SNR situation based on their unique high performance peculiarity in the above condition. Moreover, the proposed methods are capable of ensuring satisfactory performance even in snapshot-limited (high-variability) scenarios, whereas MUSIC-originated methods require a considerably-higher number of snapshots, as evident from Figure 8.

(**a**)
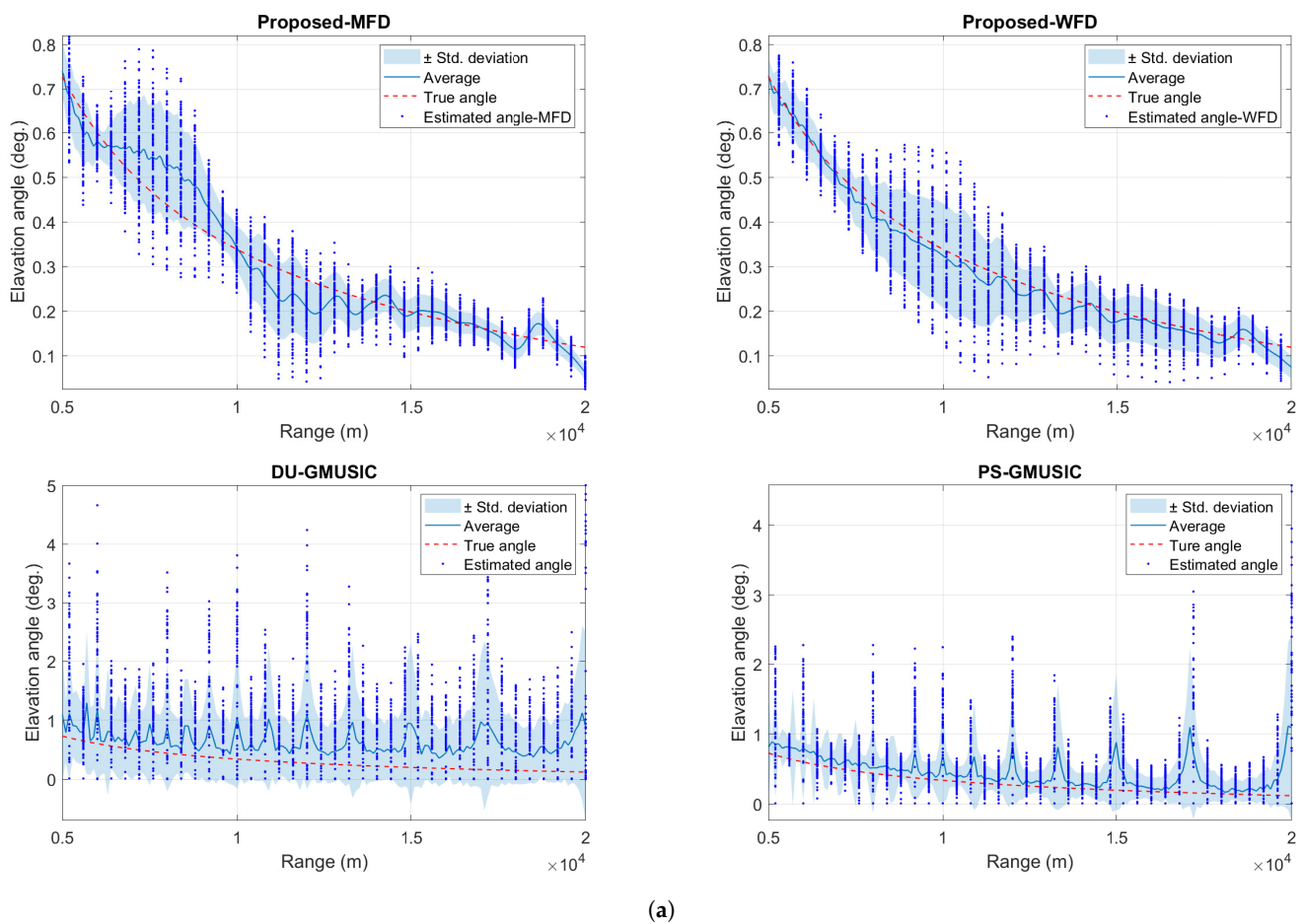
Figure 5. *Cont.*
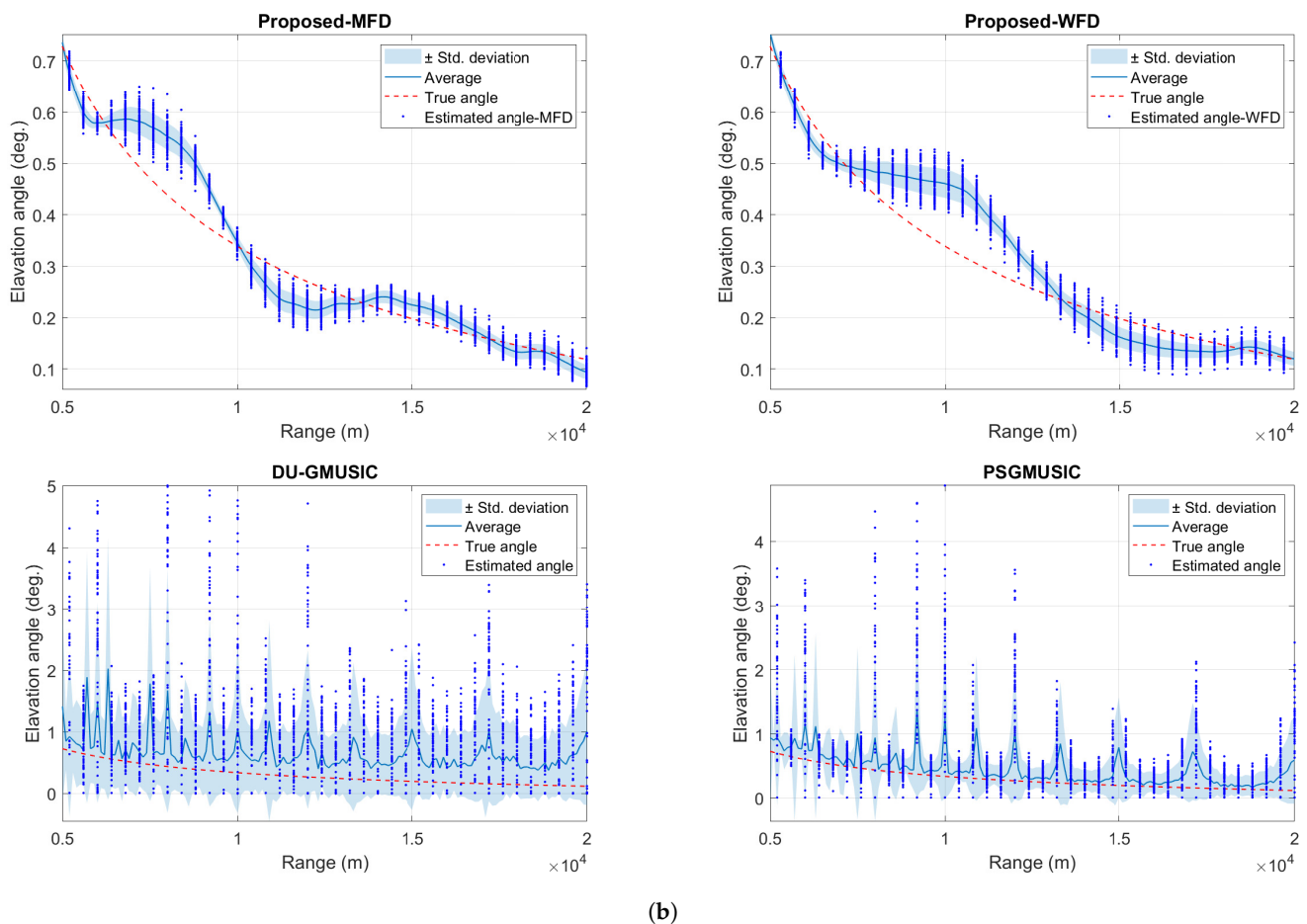
Figure 5. Scatter graph of the elevation angle estimates vs. the range (in meters). The plot highlight the bias-variance decomposition of the considered estimators. Specifically, the difference between the (solid) blue and (dashed) red lines underlines the estimator bias. Conversely, the shaded area corresponds to ± std. deviation, providing an indication of the estimator variance. (**a**) Smooth surface. (**b**) Rough surface.

Furthermore, to assess the stability of the proposed trackers to non-nominal conditions, the impact of the mismatch of observation noise variance σ_c^2 between measurements and EKF is assessed in Figure 9. In the above case, a mismatch factor ϵ is considered in the observation noise covariance matrix (i.e., $C = \epsilon \sigma_c^2 I_N$) within the EKF. As expected, Figure 9 reveals that a high value of the mismatch factor has a slight negative impact on the proposed method overall performance and that the proposed method is strongly robust against observation noise mismatch over both FD algorithms.

Interestingly, in the rough surface scenario, the proposed method exhibits a higher performance over undervalued mismatches (i.e., below 10^0). This mainly occurs since reducing the mismatch factor implies that the EKF is weighting more the correction step than the prediction step (cf. Equations (24) and (35)), which, for the rough surface scenario, better represents the observation noise due to random behavior of the diffuse component.

Finally, Figure 10 shows the RMSE of the target elevation angle estimate against the RMS of the surface roughness (σ_h). The performance results are reported for both the proposed approaches and the considered MUSIC-based baselines. As expected, the RMSE of the proposed methods are significantly lower in different multipath situation, especially for high values of σ_h.
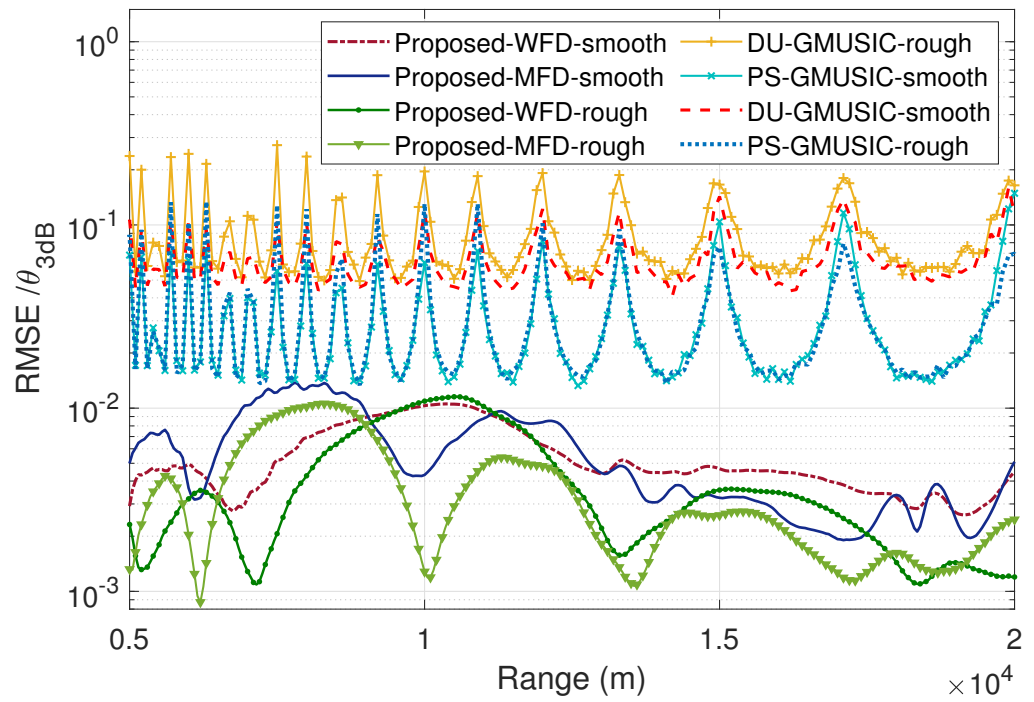
Figure 6. RMSE of elevation angle estimation (θ_t) vs. the target range.
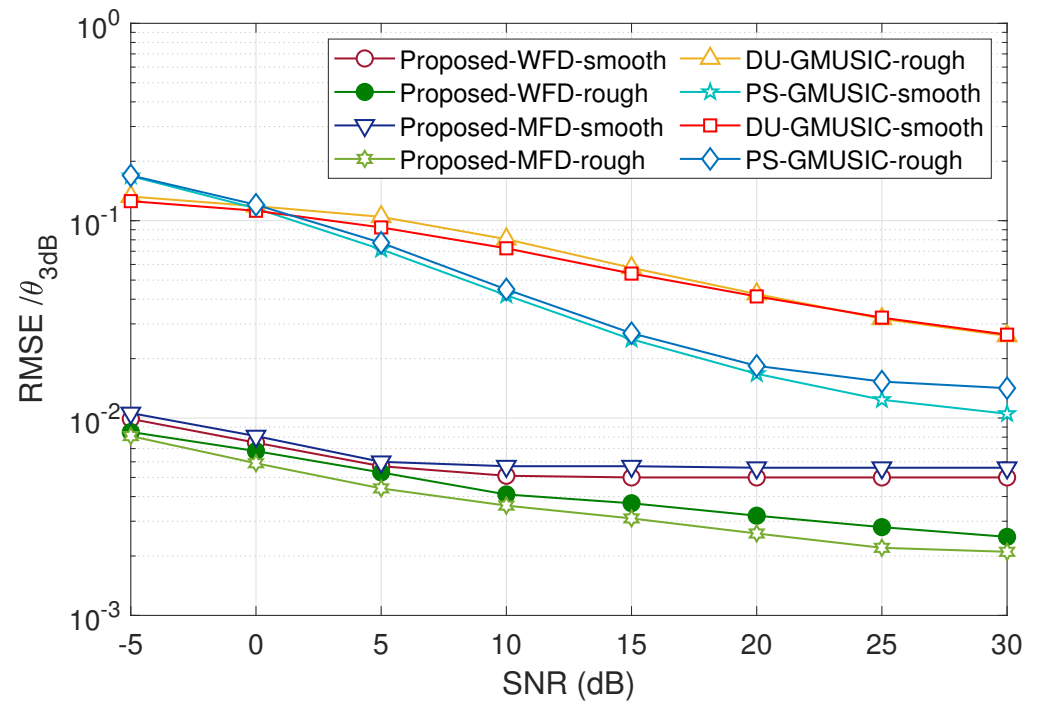
Figure 7. RMSE of the target elevation angle (θ_t) against the SNR.
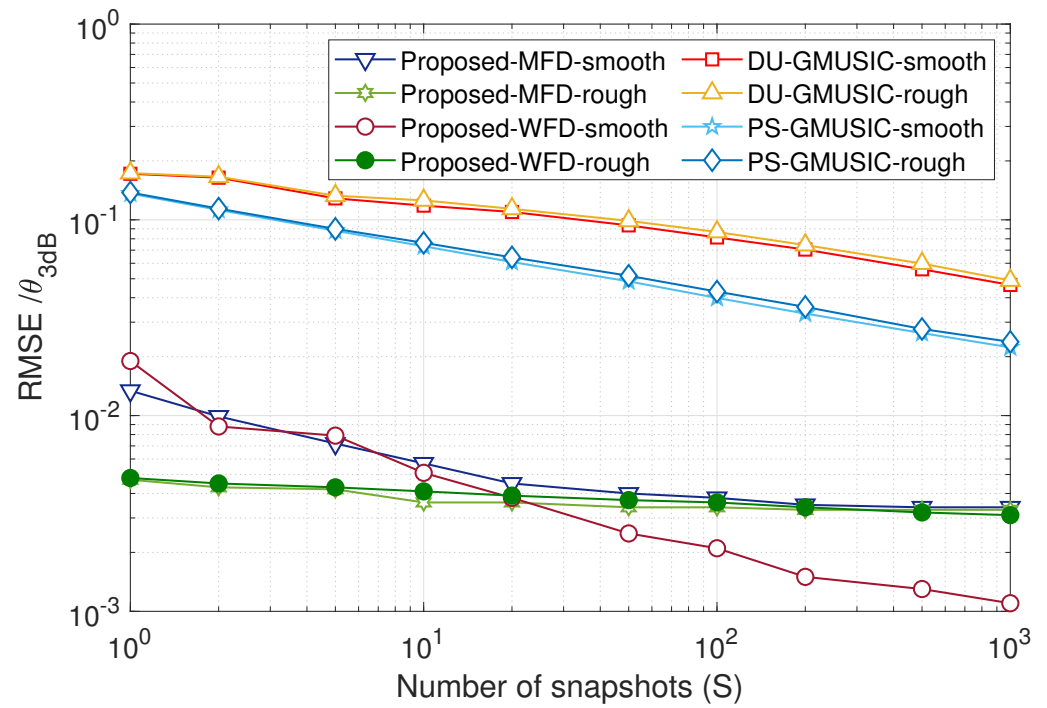
Figure 8. RMSE of the target elevation angle (θ_t) against the number of snapshots.
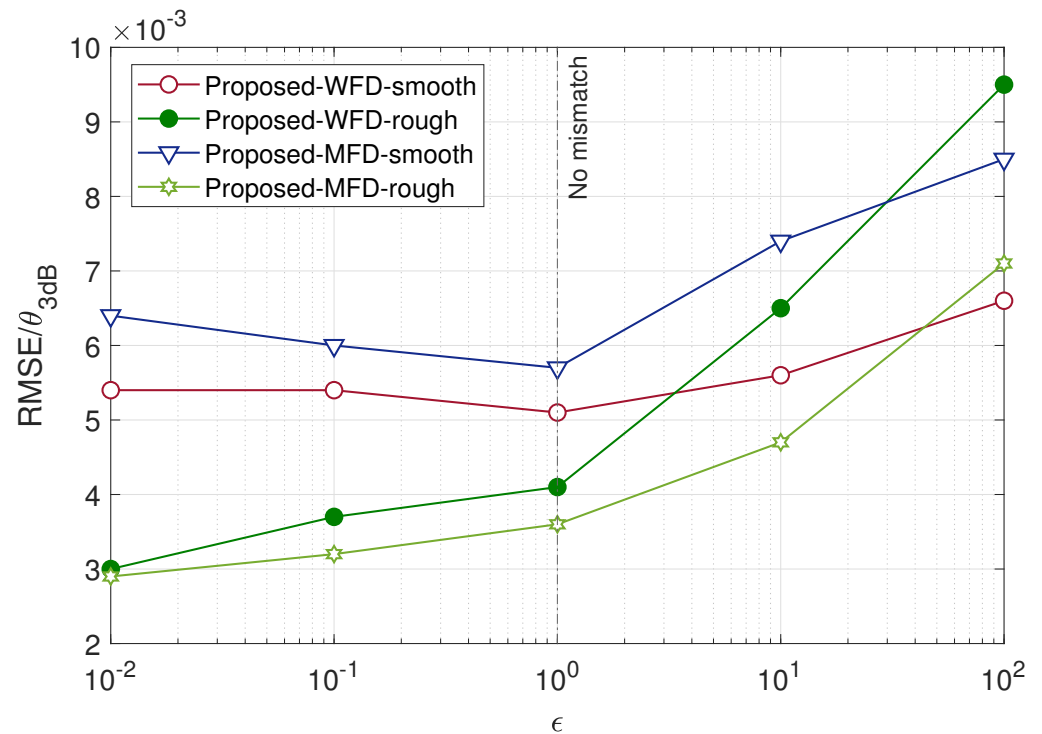
Figure 9. RMSE of the target elevation angle (θ_t) in the presence of a mismatch factor ϵ. In the above plot, $\epsilon = 1$ refers to the "no-mismatch" case, as highlighted in the figure via a dashed vertical line.
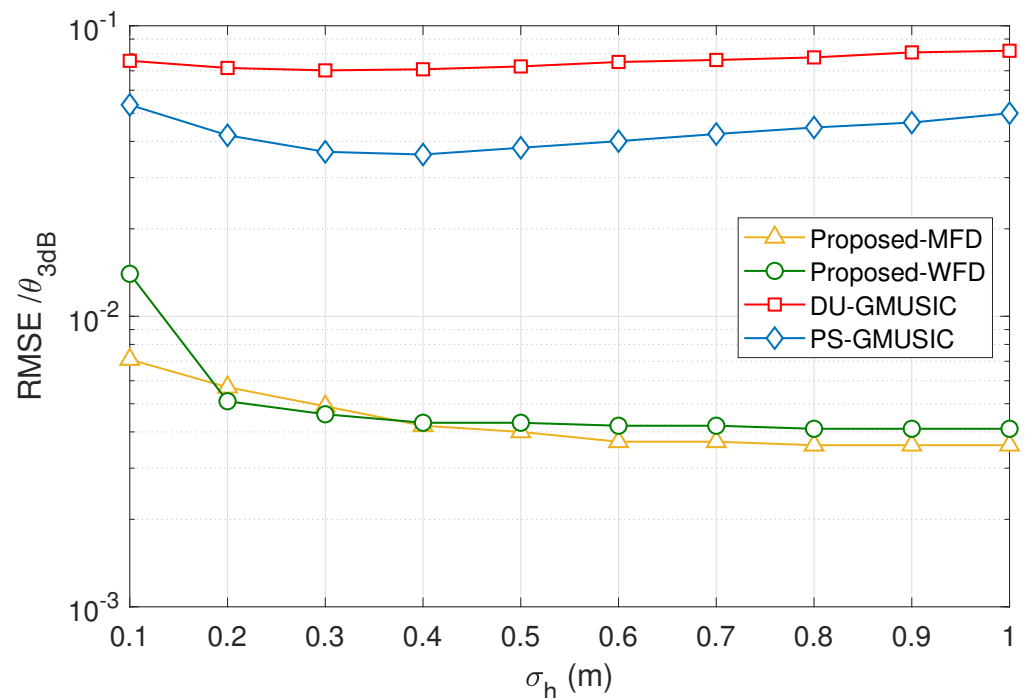
Figure 10. RMSE of the target elevation angle (θ_t) against the RMS of the surface roughness (σ_h).

5. Conclusions and Future Directions

In this paper, we tackled the problem of low-angle isolated-target tracking in multipath environments. Specifically, we proposed an elevation angle estimation method via the EKF and promoted this method by two FD processes. Our method does not require any additional prior knowledge of geometrical information and physical parameters and, equally important, enjoys a low computational load. The simulation results showed that the proposed methods have a precise (close) elevation angle estimation in any multipath situation whereas the considered baselines (i.e., DU-GMUSIC and PS-GMUSIC methods) are not able to track the target accurately.

Indeed, due to the EKF properties and the proposed FD processes, our approaches are able to considerably suppress the diffuse and specular components, thus, mitigating their corresponding fluctuations. Both proposed methods maintain their excellent performance even in very-low SNR situation, while the performance of many other relevant methods drops off significantly. These methods can be used in the low probability of intercept or low-peak-power radars due to their high performance in very low SNR. Future works will account for multiple-target tracking in the considered setup, privacy issues associated to tracking estimates [35] and assessing the performance of the proposed approaches with real data.

Author Contributions: Conceptualization, H.D. and D.C.; Methodology, H.D. and M.A.S.; Supervision, M.A.S. and P.S.R.; Validation, D.C.; Writing—original draft, H.D.; Writing—review and editing, D.C. and P.S.R. All authors have read and agreed to the published version of the manuscript.

Institutional Review Board Statement: Not applicable.

Informed Consent Statement: Not applicable.

Data Availability Statement: Not applicable.

Abbreviations

The following abbreviations are used in this manuscript:

AoA	Angle of Arrival
DN	Double Null
(E)KF	(Extended) Kalman Filter
FB	Fixed Beam
LS	Least Squares
(G)MUSIC	(Generalized) Multiple Signal Classification
DU-GMUSIC	Double Unitary transform based GMUSIC
PS-GMUSIC	Polarization Smoothing GMUSIC
(Q)(R)ML	(Quadrature) (Refined) Maximum Likelihood
RMS(E)	Root Mean Square (Error)
SNR	Signal-to-Noise Ratio
ULA	Uniform Linear Array
(W/M)FD	(Weighted/Matrix-based) Frequency Diversity

References

1. White, W.D. Low-angle radar tracking in the presence of multipath. *IEEE Trans. Aerosp. Electron. Syst.* **1974**, *AES-10*, 835–852. [CrossRef]
2. Sebt, M.A.; Sheikhi, A.; Nayebi, M.M. Robust low-angle estimation by an array radar. *IET Radar Sonar Navig.* **2010**, *4*, 780–790. [CrossRef]
3. Xu, Z.; Xiong, Z.; Wu, J.; Xiao, S. Symmetrical difference pattern monopulse for low-angle tracking with array radar. *IEEE Trans. Aerosp. Electron. Syst.* **2016**, *52*, 2676–2684. [CrossRef]
4. Mangulis, V. Frequency diversity in low-angle radar tracking. *IEEE Trans. Aerosp. Electron. Syst.* **1981**, *AES-17*, 149–153. [CrossRef]
5. Goodarzi, M.; Sebt, M.A.; Darvishi, H. Target and Image Elevation Angles Separation Algorithm for Low-Angle Tracking with Monopulse Antenna. In Proceedings of the 28th Iranian Conference on Electrical Engineering (ICEE), Tabriz, Iran, 4–6 August 2020; pp. 1–4.
6. Park, D.; Yang, E.; Ahn, S.; Chun, J. Adaptive beamforming for low-angle target tracking under multipath interference. *IEEE Trans. Aerosp. Electron. Syst.* **2014**, *50*, 2564–2577. [CrossRef]
7. Darvishi, H.; Sebt, M.A. Low Elevation Angle Estimation Using an Iterative Array Processing Method. *J. Commun. Technol. Electron.* **2019**, *64*, 1276–1282. [CrossRef]
8. Sherman, S.M. Complex indicated angles applied to unresolved radar targets and multipath. *IEEE Trans. Aerosp. Electron. Syst.* **1971**, *AES-7*, 160–170. [CrossRef]
9. Darvishi, H.; Sebt, M.A. Adaptive hybrid method for low-angle target tracking in multipath. *IET Radar Sonar Navig.* **2018**, *12*, 931–937. [CrossRef]
10. Schmidt, R. Multiple emitter location and signal parameter estimation. *IEEE Trans. Antennas Propag.* **1986**, *34*, 276–280. [CrossRef]
11. Tufts, D.W.; Kumaresan, R. Estimation of frequencies of multiple sinusoids: Making linear prediction perform like maximum likelihood. *Proc. IEEE* **1982**, *70*, 975–989. [CrossRef]
12. Kumaresan, R.; Tufts, R.W. Estimating the angles of arrival of multiple plane waves. *IEEE Trans. Aerosp. Electron. Syst.* **1983**, *AES-19*, 134–139. [CrossRef]
13. Qi, C.; Chen, Z.; Wang, Y.; Zhang, Y. DOA estimation for coherent sources in unknown nonuniform noise fields. *IEEE Trans. Aerosp. Electron. Syst.* **2007**, *43*, 1195–1204.
14. Xu, Z.H.; Wu, J.N.; Xiong, Z.; Xiao, S.P. Low-angle tracking algorithm using polarisation sensitive array for very-high frequency radar. *IET Radar Sonar Navig.* **2014**, *8*, 1035–1041. [CrossRef]
15. Liu, Z.; Wang, Y.; Cao, Y. Real-domain GMUSIC algorithm based on unitary-transform for low-angle estimation. *BIAI J. Syst. Eng. Electron.* **2014**, *25*, 794–799. [CrossRef]
16. Tan, J.; Nie, Z. Polarization Smoothing Generalized MUSIC Algorithm with Polarization Sensitive Array for Low Angle Estimation. *Sensors* **2018**, *18*, 1534. [CrossRef] [PubMed]
17. Ziskind, I.; Wax, M. Maximum likelihood localization of multiple sources by alternating projection. *IEEE Trans. Acoust. Speech Signal Process.* **1988**, *36*, 1553–1560. [CrossRef]
18. Zoltowski, M.D.; Lee, T.S. Maximum likelihood based sensor array signal processing in the beamspace domain for low angle radar tracking. *IEEE Trans. Signal Process.* **1991**, *39*, 656–671. [CrossRef]
19. Bosse, E.; Turner, R.M.; Lecours, M. Tracking swerling fluctuating targets at low altitude over the sea. *IEEE Trans. Aerosp. Electron. Syst.* **1991**, *27*, 806–822. [CrossRef]
20. Takahashi, R.; Hirata, K.; Maniwa, H. Altitude estimation of low elevation target over the sea for surface based phased array radar. In Proceedings of the IEEE Radar Conference (RadarConf), Arlington, VA, USA, 10–14 May 2010; pp. 123–128.

21. Wang, S.; Cao, Y.; Su, H.; Wang, Y. Target and reflecting surface height joint estimation in low-angle radar. *IET Radar Sonar Navig.* **2016**, *10*, 617–623. [CrossRef]
22. Bosse, E.; Turner, R.M.; Riseborough, E.S. Model-based multifrequency array signal processing for low-angle tracking. *IEEE Trans. Aerosp. Electron. Syst.* **1995**, *31*, 194–210. [CrossRef]
23. Akhavan, S.; Bahabadi, M.A.; Norouzi, Y.; Lolaee, H. Direction of arrival estimation using array of antennas for low-altitude targets in multi-path environment. *IET Radar Sonar Navig.* **2016**, *10*, 1439–1445. [CrossRef]
24. Zhu, Y.; Zhao, Y.; Shui, P. Low-angle target tracking using frequency-agile refined maximum likelihood algorithm. *IET Radar Sonar Navig.* **2016**, *11*, 491–497. [CrossRef]
25. Zarchan, P.; Musoff, H. *Fundamentals of Kalman Filtering: A Practical Approach*, 4th ed.; American Institute of Aeronautics and Astronautics, Inc.: Reston, VA, USA, 2015.
26. Kalman, R.E. A new approach to linear filtering and prediction problems. *J. Eng.* **1960**, *82*, 35–45. [CrossRef]
27. Liu, F.; Zhao, P.; Wang, Z. EKF-Based Beam Tracking for mmWave MIMO Systems. *IEEE Commun. Lett.* **2019**, *23*, 2390–2393. [CrossRef]
28. Jawahar, A.; Rao, S.K. Modified polar extended Kalman filter (MP-EKF) for bearings-only target tracking. *Indian J. Sci. Technol.* **2016**, *9*, 1–5. [CrossRef]
29. Hehn, M.; Sippel, E.; Vossiek, M. An Iterative Extended Kalman Filter for Coherent Measurements of Incoherent Network Nodes in Positioning Systems. *IEEE Access* **2020**, *8*, 36714–36727. [CrossRef]
30. Kerr, D.E.; Goudsmit, S.A.; Linford, L.B. *Propagation of Short Radio Waves*; IET: London, UK, 1987; Volume 24.
31. Northam, D.Y. *A Stochastic Simulation of Low Grazing Angle, Forward Scatter, Over-Water Multipath Effects*; Technical Report; Naval Resaerch Lab: Washington, DC, USA, 1983.
32. Beard, C. Coherent and incoherent scattering of microwaves from the ocean. *IRE Trans. Antennas Propag.* **1961**, *9*, 470–483. [CrossRef]
33. Blair, W.D.; Brandt-Pearce, M. Statistics of monopulse measurements of Rayleigh targets in the presence of specular and diffuse multipath. In Proceedings of the IEEE Radar Conference (RadarConf), Atanta, GA, USA, 3 May 2001; pp. 369–375.
34. Kay, S.M. Volume I: Estimation Theory. In *Fundamentals of Statistical Signal Processing*; Prentice Hall: Hoboken, NJ, USA, 1993.
35. Ciuonzo, D.; Willett, P.K.; Bar-Shalom, Y. Tracking the tracker from its passive sonar ML-PDA estimates. *IEEE Trans. Aerosp. Electron. Syst.* **2014**, *50*, 573–590. [CrossRef]